Fabrication of Noncovalent and Covalent Internal Scaffolding in Monolayer Assemblies Using Diacetylenes

Henning Menzel,† Mark D. Mowery, Mei Cai, and Christine E. Evans*

Department of Chemistry, University of Michigan, Ann Arbor, Michigan 48109-1055

Received November 30, 1998

ABSTRACT: Internal molecular scaffolding is created by the lateral association of molecules at specific vertical positions within a single molecular layer. In this paper, such internal scaffolding is demonstrated for both noncovalent and covalent interactions using diacetylene-containing precursors. Previously shown to form a covalent polymer backbone upon UV irradiation, diacetylenes are shown here to also exhibit noncovalent lateral interaction prior to polymerization. Preferential twist orientation of the methylene side chains and distinct methyl group orientation illustrate the presence of this noncovalent scaffolding. Upon formation of the cross-linked polymer backbone, alkyl chain crystallinity and end group orientation are not significantly altered, but the methylene chain twist orientation is decreased. Evaluated as a function of the vertical position of the scaffolding within the monolayer, all monolayers exhibit excellent long-range order as measured by the electron-transfer properties.

Introduction

The selective control of interfacial environments utilizing the design of thin organic films has resulted in interesting new materials.[1] By combining these strategies with polymer chemistry, numerous possibilities for incorporation of molecular functions or physical properties within one material are attainable. Polydiacetylenes are particularly interesting due to the stiff and highly conjugated backbone that leads to intriguing optical and electronic properties.[2] Polydiacetylenes have the added advantage of an electronic transition in the visible region whose exact frequency is highly dependent upon the effective conjugation length of the polymer backbone. Because this effective conjugation length is strongly influenced by the local order in the vicinity of the backbone, polydiacetylene Langmuir−Blodgett (LB) films have recently been utilized in colorimetric sensor applications.[3−5] Extensively characterized as thin films and LB layers,[2,6−10] recent studies have demonstrated the feasibility of fabricating polydiacetylene monolayers in surface-attached assemblies.[11−13] Using this approach, the interfacial structure of the monolayer has been controlled through phototemplating.[12b] Recently, the vertical position of the diacetylene units has been varied synthetically, affording three-dimensional control over the molecular architecture of these monolayer assemblies.[13c] In this paper, this vertical positioning of the diacetylene within the monolayer is evaluated with respect to the internal scaffolding formed by interaction between neighboring diacetylenes before polymerization and the covalent scaffolding created after polymerization.

Generally, self-assembled monolayers that incorporate diacetylene groups have been characterized as alkanethiol monolayers with an internal functional group. However, the overall structural order of these assemblies may differ from simple alkanethiol structures due to the presence of an internal molecular scaffolding that orders the monolayer laterally. Indeed,

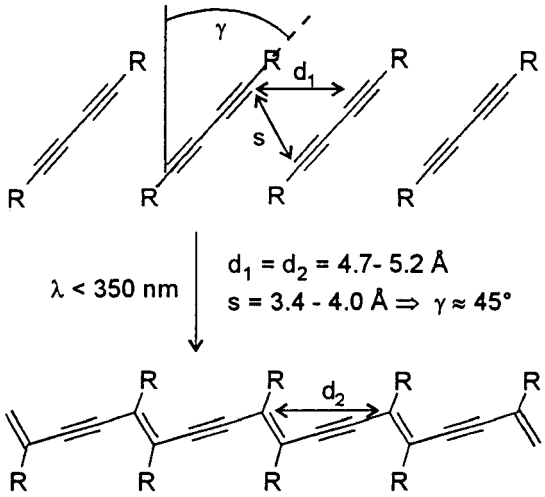

Figure 1. Steric requirements for the polymerization of diacetylenes.

the spatial proximity required for polymerization[14−16] (Figure 1) may be expected to yield significant interactions between neighboring, electron-rich diacetylene units. Such a close-packed structure of π-systems is likely to give rise to lateral association within the monolayer similar to that observed in systems showing hydrogen bonding,[17,18] π-stacking,[19,20] or dipole coupling.[21] As a result, the nonpolymerized monolayers may be expected to form a noncovalent molecular scaffolding by lateral association of adjacent diacetylene groups. In fact, recent studies of the frictional properties of these monolayer assemblies have shown discrete collapse behavior that is not observed for simple *n*-alkyl monolayers.[13e] Upon exposure to UV light, these same adjacent molecules become covalently linked within the monolayer structure. As a result, a single adsorbate can be used to fabricate both noncovalent and covalent molecular scaffolding within the same monolayer assembly.

Using this approach, monolayer structures may be considered to consist of three distinct regions: the alkyl spacer region between the surface and the diacetylene, the tail region above the diacetylene, and the diacety-

† Permanent address: Institute for Macromolecular Chemistry, University of Hannover, Am Kleinen Felde 30, D-30167 Hannover, Germany.

10.1021/ma981839q CCC: $18.00
Published on Web 06/04/1999

lene units themselves. As the vertical positions of the diacetylene units are varied within the monolayer, the resultant molecular architecture may be expected to influence the mutual interaction of the different regions in the assembly. These interactions will ultimately determine whether neigboring diacetylene units can adapt an arrangement favorable for polymerization. The formation of a molecular scaffolding within the monolayer, in turn, impacts the structure of the alkyl portions of the monolayer. For LB films incorporating diacetylene scaffolding, the interdependence between the molecular architecture and the structure and polymerizability has been well studied.[8−10] However, the analogous self-assembled monolayers (SAM) have a Au−S bond to the surface that is much stronger, and consequently, results obtained for LB films may not be directly applicable for predicting the properties of diacetylene monolayers on gold. Molecular architecture within these monomolecular assemblies is controlled synthetically by varying the position of the diacetylene groups within the alkyl chain:

$$\begin{array}{l} CH_3\text{-}(CH_2)_n\text{-}C{\equiv}C\text{-}C{\equiv}C\text{-}(CH_2)_m\text{-}S \\ \qquad\qquad\qquad\qquad\qquad\qquad\qquad\quad | \\ CH_3\text{-}(CH_2)_n\text{-}C{\equiv}C\text{-}C{\equiv}C\text{-}(CH_2)_m\text{-}S \end{array}$$

An *n*,*m*-DA and *n*,*m*-PDA designation is used to identify the nonpolymerized and the polymerized monolayer architectures, respectively, with *n* giving the number of methylene units in the tail region and *m* the number of methylene units in the spacer region. The structure of these monolayers is examined both with the noncovalent scaffolding and after exposure to UV light yields the covalently linked molecular assembly. Resonance Raman spectroscopy is used to monitor the formation of the covalent scaffolding within the monolayer assemblies upon photopolymerization. The interdependence between alkyl chain structure and the presence of noncovalent or covalent molecular scaffolding is investigated by electrochemical methods and FTIR spectroscopy.

Experimental Methods

Synthesis. Di(heneicosa-10,12-diyn)disulfide (7,9-DA), di(pentacosa-10,12-diyn)disulfide (11,9-DA), di(tetracosa-5,7-diyn)disulfide (15,4-DA), di(hexacosa-7,9-diyn)disulfide (15,6-DA), and di(nonacosa-10,12-diyn)disulfide (15,9-DA) were synthesized according to a previously described general procedure.[22] Briefly, the synthetic route comprises a Cadiot−Chodkiewicz coupling of an iodinated 1-alkyne with an ω-alkyn-1-ol for the synthesis of the diacetylene group. The 7-octyn-1-ol starting material for the synthesis of 15,6-DA is not commercially available and was synthesized according to Brown[23] by isomerization of 2-octyn-1-ol using the potassium salt of 1,3-diaminopropane.[24,25] The coupling product, a diacetylene with a terminal hydroxy group, is tosylated and subsequently treated with sodium hydrogen sulfide under sonication. This results in a mixture of the thiol and the symmetrical disulfide, which can be chromatographically purified using silica gel and hexanes/dichloromethane (4:1) as solvent. All diacetylene disulfides were white, crystalline materials which show a single spot by TLC (hexanes/dichloromethane 4:1), with no impurities observed by ^{1}H NMR. In contrast to the analogous thiols, these diacetylene-containing disulfides are quite robust and can be stored for extended periods (>12 months) without degradation or polymerization.

Monolayer Fabrication. Gold films are deposited on mica using a custom-built UHV thin-film deposition system. The mica (ASTM V-2; Asheville-Schoonmaker Mica Co.) was cleaved on both sides immediately before insertion into the chamber. The mica substrates were suspended 21 cm above the source using a tantalum mask and baked out at 380 °C for 12−24 h using two 500 W halogen lamps positioned approximately 7.5 cm below the substrate. The temperature was subsequently decreased to 250 °C, and gold (99.99%) was evaporated from a K-Cell (Oxford Instruments) onto the mica at a rate of 0.03 Å/s to a final thickness of approximately 2000 Å ($P < 1 \times 10^{-7}$ Torr). After deposition, the substrates were annealed for 1 h at the deposition temperature and then allowed to cool to room temperature ($P = 2 \times 10^{-10}$ Torr). Gold films prepared in this manner are known to contain atomically flat domains that are greater than 100 nm in diameter and are characterized by a predominance (99+%) of (111) crystallographic orientation.[26] Finally, the chamber was backfilled with dry nitrogen, and the substrates were removed, immediately immersed in a 1 mM chloroform solution of the diacetylene disulfide or octadecanethiol, and allowed to equilibrate at room temperature for 40−48 h. Strict light control was maintained during the preparation and storage of the diacetylene solutions and monolayer films. The substrates were then removed and rinsed extensively with chloroform (Aldrich; > 99%) and deionized water (model UV Plus Milli-Q, Millipore; >18 MΩ) and dried under nitrogen. The resulting diacetylene monolayers were subsequently polymerized under nitrogen with a low-intensity UV lamp (model UVG-11; Ultra-Violet Products Inc.; $\lambda = 250-260$ nm) at a distance of 2 cm. Using this procedure, no photooxidation of the Au−S bond is observed.[27a]

Raman Spectroscopy. Resonance Raman spectra were obtained using a microscope objective (10×, 0.25 NA), a spectrograph (Holoscope *f*/1.8; VPT; Kaiser Optical System), and a charge-coupled device (CCD) detector (TK1024AB, Photometrics). The 632.8 nm line from a He−Ne laser (model 05-LHP-991, Melles Griot) was utilized for excitation, with an incident laser power of 4−5 mW. The detector was cooled with liquid nitrogen to −110 °C, and spectra were calibrated using emission lines of known wavelength from a neon lamp.

Electrochemistry. Cyclic voltammetry was performed in a conventional three-electrode cell with the area of the gold working electrode (0.95 cm^2) defined by an inert elastomer O-ring. The reference and counter electrodes were a double-junction Ag/AgCl (saturated KCl) and coiled platinum electrode, respectively. A Bioanalytical Systems CV-27 potentiostat and a Hewlett-Packard XY recorder were used, and all experiments were conducted at room temperature (22 ± 1 °C). The solutions were prepared immediately before use with ultrahigh-purity deionized water (model UV Plus Milli-Q; Millipore: >18 MΩ).

Fourier Transform Infrared Spectroscopy. Grazing-angle FTIR experiments were accomplished using a nitrogen-purged Nicolet 550 Magna IR spectrometer with a liquid nitrogen cooled MCT detector. Spectra were obtained with a Spectra-Tech Inc. specular reflectance accessory using p-polarized light incident on the samples at 85° with respect to normal. All spectra were taken as the average of 1024 scans at a resolution of 2 cm^{-1} and were referenced against a freshly prepared, unmodified gold film.

Results and Discussion

Photopolymerizeable diacetylene moieties provide two different mechanisms for creating internal scaffolding within a single molecular layer. In the unpolymerized form, scaffolding is initiated solely by noncovalent interactions among electron-dense diacetylene groups on neighboring molecules. Upon polymerization, covalent scaffolding is created in the form of a highly conjugated polymer backbone. Using resonance Raman spectroscopy, the formation of the covalent scaffolding is selectively measured within the monolayer structure.[8,13b,28,29] The polymerization process itself is not expected to significantly expand or contract the monolayer.[14−16] However, as shown in Figure 1, the acetylenic

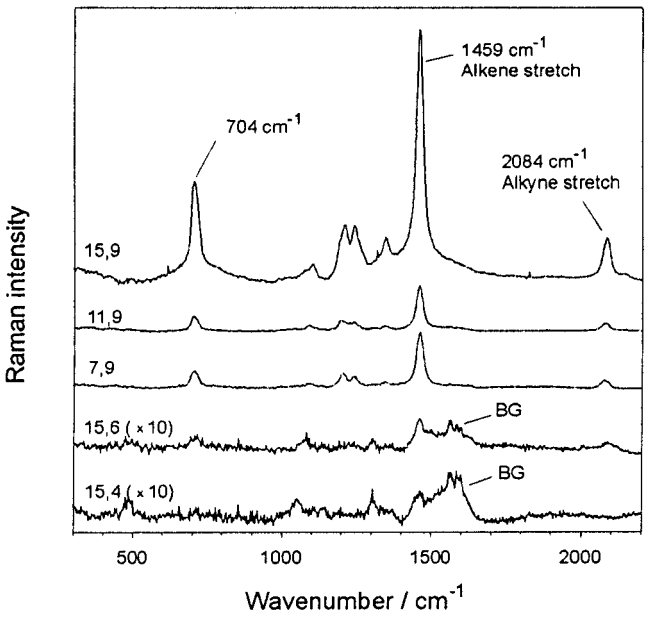

Figure 2. Resonance Raman spectra of the PDA monolayers using a wavelength of 633 nm for excitation. BG = background.

carbons at the top and bottom of the diacetylene monomers undergo a change in hybridization from sp to sp^2. Since the polymer backbone is parallel to the surface, this shift in hybridization may result in a change of the bond orientation above and below the scaffolding. In this paper, the presence of these two different scaffolding structures is assessed and their properties are evaluated.

Polymerization. Resonance Raman spectroscopy provides a good measure of polymerization in diacetylene monolayers. The highly conjugated polymer backbone contains an excitonic absorption band in the visible region. Using a resonant frequency for excitation, the Raman spectrum of the polymer backbone is enhanced, allowing selective monitoring of the polymer backbone. Indeed, under the conditions used in this study, assemblies containing unpolymerized diacetylene groups or only *n*-alkyl chains exhibit no detectable signal. As a result, the intensity of the Raman scattering originating from the alkene and alkyne stretches of the polymer backbone provides a direct measure of polymerization. The excitation frequency is chosen to be exclusively in resonance with the longest conjugation length, blue form of the polymer.[8,28] Although polymerization is observed for all precursors examined here, the molecular architecture appears to significantly affect the degree of formation of the highly conjugated polymer scaffolding (Figure 2). Resonance Raman spectra of the polymerized monolayers display peaks attributed to alkene (1460 cm^{-1}) and alkyne (2084 cm^{-1}) stretching transitions in the polymer backbone. The position of these transitions are shifted lower than expected for isolated double and triple bonds, consistent with the delocalization expected by the conjugated nature of the polymer. Significant formation of the long conjugation length polymer is observed for 15,9-PDA assemblies, with the 11,9-PDA and 7,9-PDA monolayers also displaying good polymerization. In contrast, limited formation of the long conjugation length polymer is observed in the 15,6 and 15,4 assemblies. Interestingly, recent studies show the formation of shorter conjugation length polymer for all architectures.[27]

On the basis of these observations, polymer formation appears to be highly dependent on the molecular architecture. In general, the highest degree of polymerization is observed for those monolayers with the longest alkyl spacer length. Since the spacer is more constrained than previously studied LB films, it is feasible that the longer spacer can more easily accommodate the hybridization change upon polymerization. However, in addition to the spacer length, the odd−even character of the methylene chain may play an important role in this respect. Simple modeling of the structure of an all-trans chain reveals that, for an odd-numbered spacer, an arrangement favorable for polymerization can be easily obtained with standard bond angles for the sulfur (Au−S, 1.936 Å; Au−S−C, 104°; sp^3 hybridization of the sulfur[30]). However, in the case of an even-numbered spacer, some gauche conformations in the alkyl spacer or a different anchoring (Au−S, 1.905 Å; Au−S−C, 180°; sp hybridization of the sulfur[30]) are necessary to achieve the same orientation of the diacetylene groups. The latter anchoring has been deduced from ab initio calculations for alkanethiol monolayers on gold[30] but, to the best of our knowledge, has yet to be experimentally observed. Studies are presently underway to deconvolve the odd/even character of the spacer from the distance dependence. Nonetheless, polymer formation is observed for all architectures examined here.

Long-Range Order. The inhibition of electron transfer provides a good measure of the film quality and spatial defects in self-assembled monolayers.[31−33] In this experiment, heterogeneous electron transfer is monitored in response to potential cycling in the presence of a redox species. In the ideal case, access to the underlying gold surface is completely inhibited by the monolayer, and the cyclic voltammogram may exhibit an exponential current increase arising from tunneling through the monolayer. In contrast, interfaces with sparse defect densities and independent radial diffusion layers at each defect are expected to exhibit a plateau in the voltammetric curve. At higher defect densities, simple linear diffusion dominates, electron transfer is uninhibited, and the voltammetric curve has the characteristic peak shape.

As illustrated in Figure 3, the bare gold substrate shows uninhibited electron transfer as expected, whereas all monolayers studied exhibit considerable blocking capability. Of the unpolymerized monolayers, the greatest inhibition is shown by the 15,9-DA with an overall blocking capability consistent with the simple octadecanethiol monolayers. Interestingly, all other unpolymerized monolayers exhibit considerable blocking capability with an apparently significant capacitive component. This observation is somewhat unusual and may indicate that small ion transport through these layers is feasible but larger ions are inhibited. If this hypothesis is true, the molecular architecture of these monolayer assemblies could be used to control the size of ions detected at the interface. Upon polymerization, an apparent decrease in the tunneling behavior through the 15,9 monolayer is observed, together with a loss in the capacitive component of the 7,9 and 11,9 layers. This observation is interesting given the wide range of methylene chain crystallinities observed for these varying tail length monolayers (vide infra). These molecular architectures are also shown to be the most favorable for the formation of the high conjugation length poly-

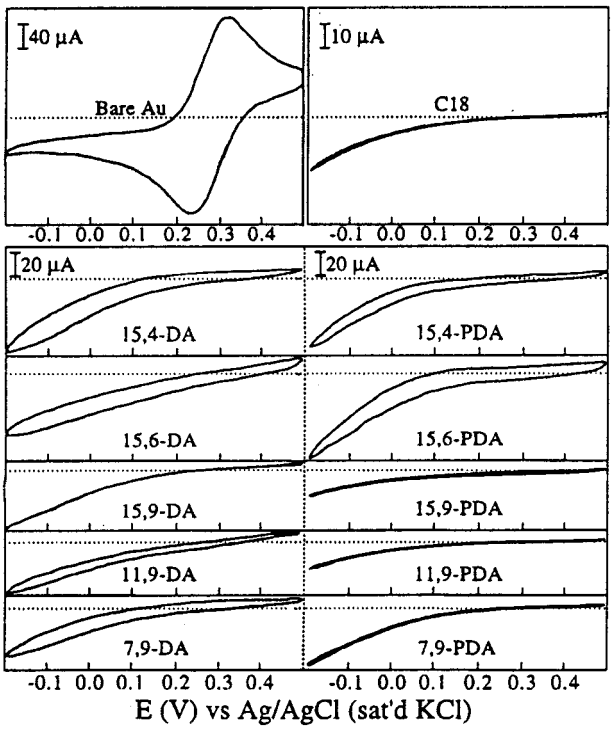

Figure 3. Cyclic voltammetric current response vs applied potential for a bare evaporated gold surface on mica and evaporated gold surfaces covered with octadecanethiol (C18), diacetylene, and polydiacetylene self-assembled monolayers. The electrolyte solution is 1.0 mM in $Fe(CN)_6^{3-}$ and 0.5 mM in KCl. The sweep rate is 100 mV/s and the temperature 22 ± 1 °C.

mer. In contrast, the shorter spacer length 15,4 and 15,6 architectures show little or no change in electron-transfer behavior upon polymerization, consistent with the minimal formation of long conjugation length polymer indicated in Figure 2. However, recent studies have shown that, although little of the extended conjugation length polymer is formed for these architectures, shorter conjugation length so-called purple and red polymer forms are observed.[27] Thus, these shorter conjugation length polymers appear to have little affect on the electron inhibition characteristics of these films, whereas formation of the longer conjugation length polymers have a notable impact on the 7,9 and 11,9 monolayers. The exact role of the polymer in the electron-transfer process remains elusive and is still the subject of investigation. These observations, however, clearly demonstrate that all molecular architectures examined here can be fabricated with a considerable degree of long-range order with noncovalent as well as covalent scaffolding.

Methylene Chain Crystallinity. The methylene chain crystallinity in self-assembled monolayers is dependent on the magnitude of the van der Waals interactions and hence the chain length. High degrees of crystallinity are observed in conventional alkanethiol monolayers when the chains are longer than approximately 12 carbons.[34] However, by incorporation of functional groups that associate laterally, the molecular scaffolding created may perturb methylene intermolecular spacings, tilt, and twist angles relative to the those observed for simple alkanethiol assemblies. In fact, the internal scaffolding can serve to divide the monolayer into distinct layers, each containing different degrees of crystallinity.[21] The influence of the diacetylene scaffolding on the monolayer crystallinity is evaluated using grazing-angle infrared spectroscopy in the C−H stretching region. The band assignments for the C−H stretching region[34−38] are summarized in Table 1 with the orientation of the transition dipole moments illustrated in Figure 4. It is important to note, however, that these measurements are ensemble averaged and will result from a convolution of the tail and spacer methylene chains.

Table 1. Band Assignment for the C−H Stretching Region of the Diacetylene Monolayers

peak position, observed, cm^{-1}	peak position, literature, cm^{-1}	mode assignment[a]	order	ref
2851	2851	$\nu_s(CH_2)$	cryst	34
2855−2860	2855		liq	34
2878	2878	$\nu_s(CH_3$, FR)		38
2918	2918	$\nu_a(CH_2)$	cryst	34
2924−2928	2928		liq	34
2935	2937	$\nu_s(CH_3$, FR)		34
~2994 (broad)	~2898 (broad)	$\nu_s(CH_2$, FR)		37
	2956	$\nu_a(CH_3$, ip)		34
2963	2965	$\nu_a(CH_3$, op)		34

[a] Mode assigment nomenclature: ν_a = asymmetric, ν_s = symmetric, FR = Fermi resonance, ip = in-plane, and op = out-of-plane.

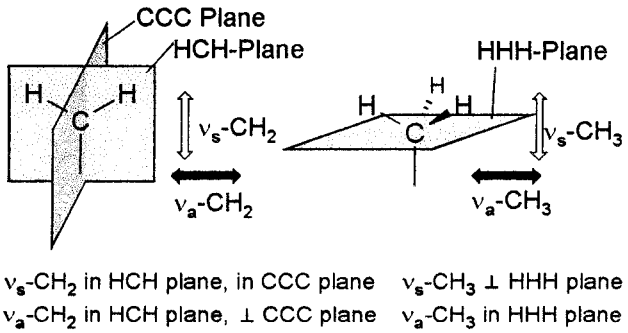

Figure 4. Schematic diagram of the molecular frame of reference for an all-trans alkyl chain at the surface with chain tilt angle, α, and twist angle, *β*, shown together with the transition moment orientations for the C−H stretching modes.

The positions of the asymmetric (ν_a-CH_2) and symmetric methylene stretching vibrations (ν_s-CH_2) are highly sensitive to the structural environment of the alkyl chains. The asymmetric and symmetric methylene stretching transitions occur at 2918 and 2850 cm^{-1}, respectively, for highly crystalline systems and increase in frequency systematically as the chains become less constrained. Spectra obtained for the diacetylene monolayer assemblies, together with an octadecanethiol monolayer, are depicted in Figure 5 with the corresponding asymmetric and symmetric stretching frequencies listed in Table 2. The peak frequencies for the unpolymerized diacetylene monolayers are clearly correlated with the molecular architecture, shifting to higher wavenumbers for those monolayers with shorter alkyl tails (11,9-DA and 7,9-DA). In contrast, no such trend is observed with decreasing spacer length (Table 2). However, a more detailed comparison of the spectra for the highly ordered diacetylene monolayers (15,9-DA, 15,6-DA, and 15,4-DA) with the octadecanethiol monolayer reveals that, although the peak position is almost identical, the peak shape varies considerably (Figure 5). For the unpolymerized diacetylene spectra, the ν_a-CH_2 and ν_s-CH_2 bands both have a component shifted to higher energy, indicated by a shoulder at higher wavenumbers. These shoulders appear at wavenumbers

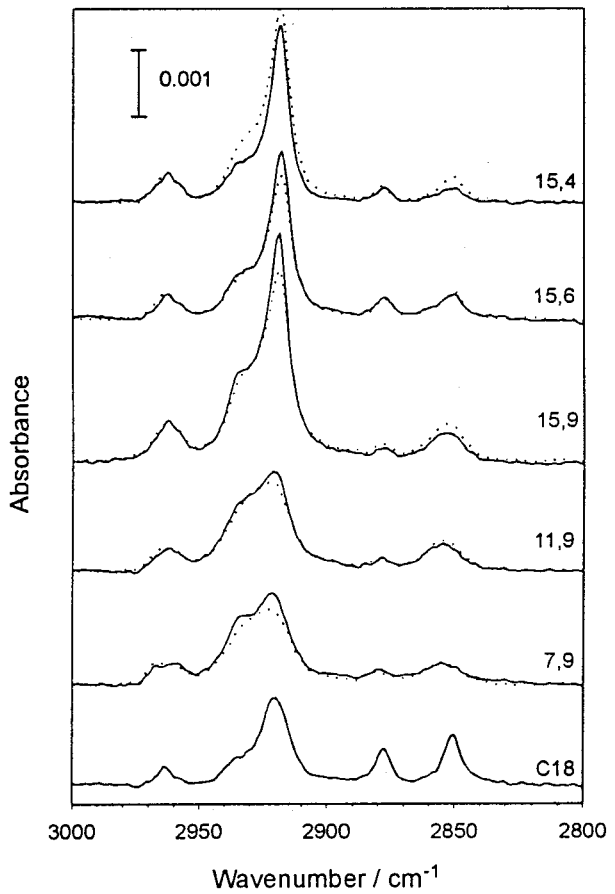

Figure 5. GIR spectra of octadecanethiol, diacetylenes (solid line), and polydiacetylenes (dotted line) as monolayers on evaporated gold surfaces.

Table 2. Observed Peak Frequencies and Intensities for the ν_a-CH_2 and the ν_s-CH_2 Bands and Their Intensity Ratio $R = I(\nu_a\text{-}CH_2)/I(\nu_s\text{-}CH_2)$ Averaged for Four Samples

monolayer	ν_a-CH_2, cm^{-1}	ν_a-CH_2 int	ν_s-CH_2, cm^{-1}	ν_s-CH_2 int	R^a
15,4 DA	2919	0.002 56	2851	0.000 28	9.7 ± 2.4
15,4 PDA	2919	0.002 56	2851	0.000 29	8.9 ± 1.3
15,6 DA	2919	0.002 43	2851	0.000 36	6.9 ± 1.1
15,6 PDA	2919	0.002 00	2851	0.000 41	4.9 ± 0.8
15,9 DA	2919	0.003 68	2852	0.000 29	13.0 ± 2.7
15,9 PDA	2919	0.002 77	2851	0.000 36	8.1 ± 2.2
11,9 DA	2924	0.001 37	2855	0.000 46	*b*
11,9 PDA	2924	0.001 22	2855	0.000 46	*b*
7,9 DA	2925	0.001 16	2855	0.000 33	*b*
7,9 PDA	2926	0.001 06	2855	0.000 37	*b*
octadecane-thiol	2920	0.001 37	2851	0.000 70	2.0 ± 0.2

[a] The error is the standard deviation of four measurements. [b] The convolution of the ordered and disordered transitions does not allow a correct calculation.

previously assigned to methylene units in a liquidlike state (Table 1),[34,38] indicating that a less constrained component is present in the methylene chains of the unpolymerized monolayers. The hypothesis of a structure with well-ordered domains accompanied by less-ordered boundaries (as proposed in ref 11) is in contrast to contact angle measurements[13c] and the electron-transfer observations. In both cases, these measurements indicate a well-ordered interfacial region with excellent long-range order. Alternatively, a model where the spacer and tail regions have different methylene chain structures is proposed. In this case, a tightly packed alkyl tail region would provide an ordered methyl surface with high blocking capability, masking a more loosely packed spacer region. Such a layered structure has been proposed previously for a dipole-coupled monolayer structure[21] and may be initiated by the lateral association of the diacetylenic units in this case. That is, the spacer may be confined between the scaffolding created by the diacetylenic groups and the Au surface, inhibiting formation a close-packed crystalline structure. It is important to note that a decreased crystallinity, as sensed by infrared spectroscopy, is not associated solely with the absence of order. In the case of the unpolymerized diacetylene monolayers, increased peak frequences would also be observed if the spacer is in an arrangement with reduced chain−chain interactions, a so-called conformationally ordered, liquid state.

The transition from a noncovalent to a covalent scaffolding is expected to further alter the structure of the alkyl chains. Although no significant expansion or contraction of the monolayer is expected,[2,14−16] the polymerization process is accompanied by a change in hybridization of the acetylenic carbons at the ends of the diacetylenic units (Figure 1). The strain induced by this change in bond angle may affect the internal structure of the monolayer. However, the data as summarized in Table 2 and Figure 5 indicate that no significant change in peak position is observed for the methylene asymmetric or symmetric stretching transitions. Thus, the methylene chain crystallinity in these monolayer structures is quite similar, regardless of the noncovalent or covalent nature of the internal scaffolding.

Tilt and Rotation of the Polymethylene Tail. Along with crystallinity information, infrared spectroscopy also provides insight into the orientation of the methylene chain. The influence of internal molecular scaffolding on the orientation of the polymethylene chains can be deduced from the relative intensities of the ν_a-CH_2 and the ν_s-CH_2 bands.[38−40] Since transition moment components that are oriented perpendicular to the gold substrate are selectively detected, insight into the ensemble averaged tilt (α) and twist (β) of the methylene chains can be determined (Figure 4). The methylene symmetric and asymmetric stretching transitions are both perpendicular to the chain axis, with ν_s-CH_2 bisecting the HCH bond angle and the ν_a-CH_2 moment oriented perpendicular to ν_s-CH_2 moment (Figure 4). Presuming an all-trans configuration, the methylene chain must have a tilt angle relative to the surface normal for either transition to be observed. In addition, some twist or rotation of the CCC plane of the methylene chain relative to the plane formed by the chain axis and the surface normal is required for the asymmetric transition to be observed. As illustrated in Figure 5 and Table 2, the large intensity of the ν_a-CH_2 band indicates a considerable tilt (and twist) of the polymethylene chain. By comparison, estimates from the C18 monolayer spectrum indicate the same or an even higher tilt angle than for conventional alkanethiols (∼30°,[34] ∼40°[38]). This observation is consistent with previous X-ray structure analysis methods of Langmuir−Blodgett multilayers of diacetylene carboxylic acids which show $\alpha = 33°$ [41] and ellipsometry measurements of similar diacetylene monolayers which indicate an $\alpha = 42°$.[12b]

In addition to the tilt angle, these monolayers also exhibit a considerable twist angle (β), as indicated by the intense asymmetric methylene stretching transition

and the relatively weak symmetric stretch. Several methods have been proposed to quantitate the ensemble average twist angle.[34,38,42,43] Among these, the spectral simulation method appears to yield the most information.[34,38,42] Unfortunately, the presence of the high-frequency shoulder on both the asymmetric and symmetric bands leads to significant errors in fitting. Estimates of the average twist angle, however, are feasible using the intensity ratio of the asymmetric to symmetric transitions. Using the projection of each transition moment onto the surface normal, the twist angle may be estimated assuming an all-trans methylene chain configuration.[43]

$$\tan\beta = \tan\beta_0\left[\left(\frac{I(\nu_a\text{-}CH_2)}{I(\nu_s\text{-}CH_2)}\right)\left(\frac{I_0(\nu_s\text{-}CH_2)}{I_0(\nu_a\text{-}CH_2)}\right)\right]^{1/2}$$

Although the high-frequency component of the stretching transitions renders even this estimate not tractable for the shorter tail architectures, estimates of the twist angle for the longest tail assemblies are feasible. Using this expression, the twist angle is approximated from the intensity ratio of the asymmetric and symmetric stretches, together with the intensity ratio for a reference SAM (denoted with a subscript 0) of known twist (β_0). Using octadecanethiol monolayers as the reference, an asymmetric-to-symmetric intensity ratio of 2.0 ± 0.2 is measured, and the twist has been determined to be $\sim 50°$.[38,42,44] This value is consistent with the twist angle expected for an isotropic distribution about the chain axis.[45] In contrast, the unpolymerized, highly ordered diacetylene monolayers (15,4-DA, 15,6-DA, and 15,9-DA) all show a much higher ratio consistent with twist angles of $\sim 65-70°$ (Table 2). Structures with such a high twist angle are indicative of a preferred orientation of the CCC plane more perpendicular to the tilt direction. Indeed, such an orientational configuration has been previously proposed for diacetylene LB films on the basis of the IR spectra[46,47] and X-ray diffraction[48] and for SAMs of alkanethiols with internal scaffolding created by dipole−dipole interactions.[21] Because the structure of the alkyl tails in the unpolymerized assemblies is comparable to the structure found in diacetylene LB films, it is likely that the structure of the tail region in the SAMs is determined more by the scaffolding created by the association of adjacent diacetylenic units than by the gold surface.

Upon polymerization, the scaffolding mechanism changes from noncovalent interactions to covalent bonding. As depicted in Figure 5 and Table 2, measurable intensity differences are observed upon polymerization for the diacetylene monolayers. Consistent with previous studies,[12b] these intensity differences can be attributed to a decrease in both the average tilt and twist of the methylene chains. Indeed, extended UV exposure studies confirm the systematic nature of the twist angle decrease with further polymerization.[27b] These apparent changes in the methylene tilt and twist angles upon polymerization may be attributed to structural changes induced by the hybridization shift. Since the polymer backbone resides parallel to the substrate, hybridization results in a decrease in the CCC bond angles above and below the backbone. In addition to decreasing the methylene chain tilt angle, this bond angle decrease may also induce a torque force on the methylene chain leading to a change in the average twist angle. Thus, although no changes in methylene chain crystallinity

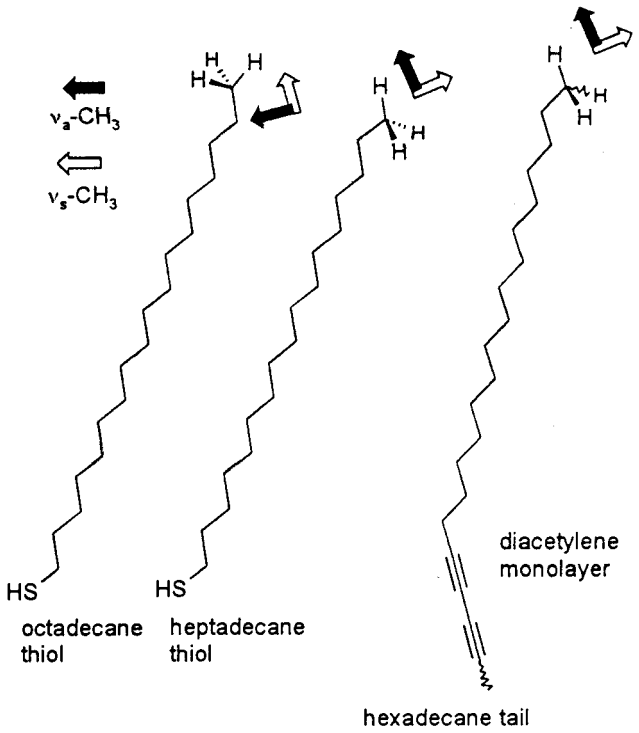

Figure 6. Schematic diagram of all-trans chains for an alkanethiols with an odd and even number of methylene units together with a diacetylene with an odd number of methylene units. Transition moment orientations for the terminal methyl groups are noted for the symmetric (open arrow) and asymmetric (dark arrow) stretching transitions.

are observed upon polymerization, both the tilt and twist of the methylene chains are clearly affected.

End Group Orientation. For terminal methyl groups, the transition moments for the symmetric (ν_s-CH$_3$ (FR), 2878 cm^{-1}) and asymmetric (ν_a-CH$_3$, 2964 cm^{-1}) stretching bands are mutually perpendicular (Figure 4). Using surface selection rules, the relative intensities of these bands provides insight into the methyl average orientation at the air−monolayer interface. A low ν_s-CH$_3$ (FR) intensity is indicative of an average C−CH$_3$ bond orientation more parallel to the surface and should be accompanied by a more intense ν_a-CH$_3$ band. Only an average orientation of the C−CH$_3$ bond exactly parallel or perpendicular to the surface would give rise to no signal for the symmetric or asymmetric methyl stretching transitions, respectively.

The previous assertion of the noncovalent scaffolding created by association of the diacetylenic units in the unpolymerized monolayers is further supported by direct comparison of the methyl bands for the highly ordered diacetylene monolayers ($n = 15$) and the octadecanethiol monolayer. Previous studies have shown a distinct odd−even effect in the ν_a-CH$_3$/ν_s-CH$_3$ (FR) intensity ratio for alkanethiols of different chain length on gold.[42] The alkanethiols with an even number of methylene units show a low ν_s-CH$_3$ (FR) intensity, i.e., a more parallel orientation of the C−CH$_3$ bond, whereas those with an odd number of methylene units show a stronger ν_s-CH$_3$ band, i.e., a more perpendicular orientation of the C−CH$_3$ bond (Figure 6). In contrast, the highly ordered unpolymerized diacetylene monolayers with an odd number of methylene units in the tail region (15,4-DA, 15,6-DA, and 15,9-DA) all show weak ν_s-CH$_3$ (FR) bands (Table 3), indicating an average orientation of the C−CH$_3$ bond that is more parallel to the surface

Table 3. Ratio $R = \nu_a\text{-}CH_3/\nu_s\text{-}CH_3$(FR) for Diacetylene R_{DA} and Polydiacetylene R_{PDA} Monolayers on Evaporated Gold Surfaces[a]

sample	R_{DA}	R_{PDA}
15,4	2.3 ± 0.4	2.3 ± 0.3
15,6	1.7 ± 0.4	1.7 ± 0.5
15,9	3.4 ± 0.5	2.7 ± 0.8
11,9	4.7 ± 2	2.2 ± 0.1[b]
7,9	3.3 ± 2	3.7 ± 2.4
octadecanethiol	0.7 ± 0.1	

[a] The error is the standard deviation of four measurements. [b] Replicate of two measurements due to minimal ν_s signal.

(Figure 6). Although some differences are observed between the 15,9-DA and the 15,4 and 15,6 monolayers, all of the long tail assemblies exhibit stretching ratios (R) that are significantly greater than expected based on a simple, alkanethiol monolayer with an odd number of methylene units. (Table 3) This preferential orientation of the terminal methyl groups is also observed for the odd-tail length 11,9 and 7,9 assemblies. However, these architectures have already been shown to have a significant component of the methylene chains that is less ordered. This likely leads to the broadening of the methyl transitions due to the wider range of orientations accessible. As a result, the methyl stretching transitions have lower intensity and concomitantly higher measurement error. Nonetheless, the methyl stretching ratio indicates the more perpendicular orientation observed for the other diacetylene architectures. Since the methylene tilt angle is similar between the diacetylene and *n*-alkyl systems (vide supra), significant differences in the methyl stretching ratio likely arise from the diacetylenes providing an anchoring point for the methylene tail that is distinct from that to the gold surface, regardless of spacer length. In fact, the anchoring angle for the carbon attached directly to the diacetylene is ~45°, whereas the carbon attached to the sulfur is ~76° (with respect to surface normal). This difference in bond angle is apparently sufficient to lead to the marked differences in end group orientation with methylene chain length when diacetylenes are present within the monolayer assembly.

As illustrated in Table 3, the change from noncovalent to covalent scaffolding upon polymerization has only a modest effect on the orientation of the methyl end groups. Consistent with the limited polymerization efficiency for the 15,4 and 15,6 structures (Figure 2), little or no change is observed upon cross-linking. The 15,9 architecture, however, exhibits a modest decrease in the methyl intensity ratio, indicating a small reorientation of the methyl groups to a more perpendicular geometry. This observation is consistent with a small decrease in the methylene tilt angle induced by changes in the hybridization and associated bond angles during polymerization. Unfortunately, the influence of cross-linking is not distinguishable for the 7,9 or 11,9 architectures due to the greater error. Although only a modest change is observed upon polymerization, the presence of both the noncovalent and covalent scaffolding within the monolayer appears to have a significant impact on the terminal group orientation.

Conclusions

In this study, diacetylene-containing alkyl disulfides were assembled onto gold surfaces to assess the formation of both noncovalent and covalent scaffolding within a single molecular layer. A strong interdependence between methylene chain structure and the formation of both noncovalent and covalent molecular scaffolding is demonstrated. High-quality assemblies with excellent long-range order are observed before polymerization, regardless of the position of the diacetylene group along the alkyl chain length. Additional improvements in barrier properties are observed when long conjugation length polydiacetylene structures are present. On a shorter scale, the order of the methylene side chains is intricately connected with the creation of internal scaffolding, with at least two distinct regions of varying degrees of crystallinity detected spectroscopically. Prior to polymerization, the methylene chains adopt a preferred orientation with a high average twist angle of the CCC plane more perpendicular to the tilt direction. Upon polymerization, a hybridization change must be accommodated at the point of the polymethylene chain attachment to the covalent scaffolding. Although this change does not impact the overall crystallinity, a clear decrease in the average twist angle is observed for the monolayer with the highest degree of polymerization. As a whole, the feasibility of controlling the properties of monolayer assemblies by exploiting the relationships between alkyl chain structure and internal scaffolding is demonstrated. Understanding how the polymer backbone is impacted by the localized methylene chain structure is crucial for applications utilizing the unique optical and electronic properties of these highly conjugated polymer interfaces.

Acknowledgment. The authors acknowledge financial support by the National Institute of General Medicine Sciences, National Institute of Health (#GM52555-01 A1). H.M. thanks the Fulbright Commision for a travel grant.

References and Notes

(1) Ulman, A. *An Introduction to Ultrathin Organic Films−From Langmuir−Blodgett to Self-Assembly*; Academic Press: San Diego, 1991 and references therein.
(2) (a) *Polydiacetylenes*; Bloor, D., Chance, R. R., Eds.; Nijhoff: Dordrecht, The Netherlands, 1985. (b) Schott, M.; Wegner, G. In *Nonlinear Optical Properties of Organic Molecules and Crystals*; Chemla, D. S., Zyss, J., Eds.; Academic Press: Orlando, 1987; Chapter 3.
(3) Charych, D. H.; Nagy, J. O.; Spevak, W.; Bedvarski, M. D. *Science* **1993**, *261*, 585.
(4) Pan, J.; Charych, D. *Langmuir* **1997**, *13*, 1365.
(5) Cheng, Q.; Stevens, R. C. *Adv. Mater.* **1997**, *9*, 481.
(6) Tieke, B.; Graf, H. J.; Wegner, G.; Naegele, B.; Ringsdorf, H.; Bauerjie, A.; Day, D.; Lando, J. B. *Colloid Polym. Sci.* **1977**, *255*, 521.
(7) Day, D.; Lando, J. B. *Macromolecules* **1980**, *13*, 1478.
(8) Tieke, B.; Lieser, G. *J. Colloid Interface Sci.* **1982**, *88*, 471.
(9) Tieke, B.; Bloor, D.; Young, R. J. *J. Mater. Sci.* (*London*) **1982**, *17*, 1156.
(10) Tieke, B. *Adv. Polym. Sci.* **1985**, *71*, 79.
(11) Batchelder, D. N.; Evans, S. D.; Freeman, T. L.; Häussling, L.; Ringsdorf, H.; Wolf, H. *J. Am. Chem. Soc.* **1994**, *116*, 1050.
(12) (a) Chan, K. C.; Kim, T.; Schoer, J. K.; Crooks, R. M. *J. Am. Chem. Soc.* **1995**, *117*, 5875. (b) Kim, T.; Ye, Q.; Sun, L.; Chan, K. C.; Crooks, R. M. *Langmuir* **1996**, *12*, 6065. (c) Kim, T.; Chan, K. C.; Crooks, R. C. *J. Am. Chem. Soc.* **1997**, *119*, 189.
(13) (a) Mowery, M. D.; Evans, C. E. *J. Phys. Chem. B* **1997**, *101*, 8513. (b) Mowery, M. D.; Menzel, H.; Cai, M.; Evans, C. E. *Langmuir* **1998**, *14*, 5594. (c) Menzel, H.; Mowery, M. D.; Cai, M.; Evans, C. E. *J. Phys. Chem. B* **1998**, *102*, 9550. (d) Menzel, H.; Mowery, M. D.; Cai, M.; Evans, C. E. *Adv. Mater.* **1999**, *11*, 131.
(14) Enkelmann, V. *Adv. Polym. Sci.* **1984**, *63*, 91.
(15) Guillet, J. *Polymer Photophysics and Photochemistry*; Cambridge University Press: Cambridge, 1987.
(16) Cao, G.; Mallouk, T. E. *J. Solid State Chem.* **1991**, *94*, 59.
(17) Clegg, R. S.; Hutchinson, J. E. *Langmuir* **1996**, *12*, 5239.

(18) Sabapathy, R. C.; Bhattacharyya, S.; Leavy, M. C.; Cleland, W. E.; Hussey, C. L. *Langmuir* **1998**, *14*, 124.
(19) Dhirani, A.; Zehner, R. W.; Hsung, R. P.; Guyot-Sionnest, P.; Sita, L. R. *J. Am. Chem. Soc.* **1996**, *118*, 3319.
(20) Sachs, S. B.; Dudek, S. P.; Hsung, R. P.; Sita, L. R.; Small, J. F.; Newton, M. D.; Feldberg, S. W.; Chidsey, C. E. D. *J. Am. Chem. Soc.* **1997**, *119*, 19563.
(21) Evans, S. D.; Goppert-Berarducci, K. E.; Urankar, E.; Gerenser, L. J.; Ulman, A. *Langmuir* **1991**, *7*, 2700.
(22) Mowery, M. D.; Evans, C. E. *Tetrahedron Lett.* **1997**, *38*, 11.
(23) Brown, C. A.; Yamashita, A. *J. Chem. Soc., Chem. Commun.* **1976**, 959.
(24) Brown, C. A. *J. Org. Chem.* **1974**, *39*, 3913.
(25) Kimmel, T.; Becker, D. *J. Org. Chem.* **1984**, *49*, 2494.
(26) (a) Liu, Z. H.; Brown, N. M. D. *Thin Solid Films* **1997**, *300*, 84. (b) Buchholz, S.; Fuchs, H.; Rabe, J. P. *J. Vac. Sci. Technol. B* **1991**, *9*, 857. (c) DeRose, J. A.; Thundat, T.; Nagahara, L. A.; Lindsay, S. M. *Surf. Sci.* **1991**, *256*, 102. (d) Putnam, A.; Blackford, B. L.; Jericho, M. H.; Watanbe, M. O. *Surf. Sci.* **1989**, *217*, 276. (e) Chidsey, C. E. D.; Loiacono, D. N.; Sleator, T.; Nakahara, S. *Surf. Sci.* **1988**, *200*, 45. (f) Salmeron, M.; Kaufman, D. S.; Marchon, B.; Ferrer, S. *Appl. Surf. Sci.* **1987**, *28*, 279.
(27) (a) Cai, M.; Mowery, M. D.; Menzel, H.; Evans, C. E. *Langmuir* **1999**, *15*, 1215. (b) Cai, M.; Mowery, M. D.; Menzel, H.; Evans, C. E. *Appl. Spectrosc.*, submitted.
(28) Tieke, B.; Bloor, D. N. *Makromol. Chem.* **1979**, *180*, 2275.
(29) Batchelder, D. N.; Bloor, D. In *Advances in Infrared and Raman Spectroscopy*; Clark, R. J. H., Hester, R. E., Eds.; Wiley: Heyden, 1984; Vol. 11, Chapter 4.
(30) Sellers, H.; Ulman, A.; Shnidman, Y.; Eilers, J. E. *J. Am. Chem. Soc.* **1993**, *115*, 9389.
(31) Amatore, C.; Savéant, J.-M.; Tessier, D. *J. Electroanal. Chem.* **1983**, *147*, 39.
(32) Bilewicz, R.; Majda, M. *Langmuir* **1991**, *7*, 2794.
(33) Chailapakul, O.; Crooks, R. M. *Langmuir* **1993**, *9*, 884.
(34) Porter, M. D.; Bright, T. B.; Allara, D. L.; Chidsey, C. E. D. *J. Am. Chem. Soc.* **1987**, *109*, 3559.
(35) Snyder, R. G.; Hsu, S. L.; Krimm, S. *Spectrochim. Acta, Part A* **1978**, *34*, 395.
(36) Snyder, R. G.; Scherrer, J. R. *J. Chem. Phys.* **1979**, *71*, 3221.
(37) Golden, W. G.; Snyder, C. D.; Smith, B. *J. Phys. Chem.* **1982**, *86*, 4675.
(38) Nuzzo, R. G.; Dubois, L. H.; Allara, D. L. *J. Am. Chem. Soc.* **1990**, *112*, 2, 558.
(39) Nuzzo, R. G.; Fusco, F. A.; Allara, D. L. *J. Am. Chem. Soc.* **1987**, *109*, 1358.
(40) Schoondorp, M. A.; Schouten, A. J.; Hulshof, J. B. E.; Feringa, B. L. *Langmuir* **1992**, *8*, 1825.
(41) Walsh, S. P.; Lando, J. B. *Mol. Cryst. Liq. Cryst.* **1994**, *240*, 201.
(42) Laibinis, P. E.; Whitesides, G. M.; Allara, D. L.; Tao, Y.-T.; Parikh, A. N.; Nuzzo, R. G. *J. Am. Chem. Soc.* **1991**, *113*, 7152.
(43) Hou, Z.; Abbott, N. L.; Stroeve, P. *Langmuir* **1998**, *14*, 3287.
(44) Terrill, R. H.; Tanzer, T. A.; Bohn, P. W. *Langmuir* **1998**, *14*, 845.
(45) Snyder, R. G. *J. Chem. Phys.* **1965**, *42*, 1744.
(46) Walsh, S. P.; Lando, J. B. *Langmuir* **1994**, *10*, 246.
(47) Werkman, P. J.; Wieringa, R. H.; Schouten, A. J. *Langmuir* **1997**, *13*, 6755.
(48) Day, D.; Lando, J. B. *Macromolecules* **1980**, *13*, 1483.

MA981839Q